Journal of Controlled Release 343 (2022) 31–42

Contents lists available at ScienceDirect

Journal of Controlled Release

journal homepage: www.elsevier.com/locate/jconrel

An automated all-in-one system for carbohydrate tracking, glucose monitoring, and insulin delivery

Hen-Wei Huang [a,b,c,1], Siheng Sean You [b,c,1], Luca Di Tizio [a,1], Canchen Li [c,1], Erin Raftery [b], Claas Ehmke [c], Christoph Steiger [b,c], Junwei Li [b,c], Adam Wentworth [b,c], Ian Ballinger [b], Declan Gwynne [a,b,c], Kewang Nan [a], Jia Y. Liang [a,b], Jason Li [b,c], James D. Byrne [a,b,c], Joy Collins [b,c], Siddartha Tamang [c], Keiko Ishida [c], Florencia Halperin [d], Giovanni Traverso [a,b,*]

[a] Department of Mechanical Engineering, Massachusetts Institute of Technology, Cambridge, MA 02139, USA
[b] Division of Gastroenterology, Brigham and Women's Hospital, Harvard Medical School, Boston, MA 02115, USA
[c] Koch Institute for Integrative Cancer Research, Massachusetts Institute of Technology, Cambridge, MA 02139, USA
[d] Division of Endocrinology, Brigham and Women's Hospital, Harvard Medical School, Boston, MA 02115, USA

A B S T R A C T

Glycemic control through titration of insulin dosing remains the mainstay of diabetes mellitus treatment. Insulin therapy is generally divided into dosing with long- and short-acting insulin, where long-acting insulin provides basal coverage and short-acting insulin supports glycemic excursions associated with eating. The dosing of short-acting insulin often involves several steps for the user including blood glucose measurement and integration of potential carbohydrate loads to inform safe and appropriate dosing. The significant burden placed on the user for blood glucose measurement and effective carbohydrate counting can manifest in substantial effects on adherence. Through the application of computer vision, we have developed a smartphone-based system that is able to detect the carbohydrate load of food by simply taking a single image of the food and converting that information into a required insulin dose by incorporating a blood glucose measurement. Moreover, we report the development of comprehensive all-in-one insulin delivery systems that streamline all operations that peripheral devices require for safe insulin administration, which in turn significantly reduces the complexity and time required for titration of insulin. The development of an autonomous system that supports maximum ease and accuracy of insulin dosing will transform our ability to more effectively support patients with diabetes.

1. Introduction

Diabetes mellitus is a chronic disease that affects 34 million people in the US and 422 million people worldwide with rapidly increasing incidence rates (1,2). It is associated with significant morbidity and is one of the top ten leading causes of death worldwide (3). Glycemic control is a primary goal of therapy in diabetes, as it reduces complications, comorbidities, and mortality, and insulin is one of the major therapeutic classes used to achieve this. Insulin is a life-saving therapy in type 1 diabetes and is prescribed as stand-alone or combination therapy for type 2 diabetes, with approximately 25% of people with diabetes using insulin (4,5). Insulin use for glycemic control involves not only self-injections, often multiple times per day, but also routine monitoring of glucose levels, most commonly from finger stick capillary blood self-sampling. Moreover, optimal insulin regimens can be extremely complex. A long-acting basal insulin is generally prescribed as a fixed dose taken once or twice daily. A different, short-acting, insulin can be used as a bolus both to mitigate the blood glucose rise after carbohydrate intake and as a correction for glucose levels above target (6).

The insulin amount that dampens the glycemic excursion from a carbohydrate load is either taken as a fixed dose, or based on an insulin-to-carbohydrate ratio prescription which offers more precision, since carbohydrate content per meal usually varies. The insulin amount needed to correct elevated glucose varies with the degree of glucose elevation and the patient's insulin resistance; it is based on an estimation of how much one unit of insulin lowers blood glucose (insulin sensitivity factor), which is specific to an individual and can even vary with the time of day (7). It has been shown clinically that the use of a bolus calculator and carbohydrate counting significantly increases the efficacy of insulin management for both type 1 and type 2 diabetes (8,9). To

Abbreviations: CGM, Continuous glucose monitoring; ILSVRC, ImageNet Large Scale Visual Recognition Challenge; PDMS, Polydimethylsiloxane; USDA, United States Department of Agriculture; CV, Cyclic voltammetry; RANSAC, Random sample consensus.

* Corresponding author at: Department of Mechanical Engineering, Massachusetts Institute of Technology, Cambridge, MA 02139, USA.
E-mail addresses: cgt20@mit.edu, ctraverso@bwh.harvard.edu (G. Traverso).

[1] These authors contributed equally.

https://doi.org/10.1016/j.jconrel.2022.01.001
Received 21 September 2021; Received in revised form 21 December 2021; Accepted 1 January 2022
Available online 6 January 2022

safely and optimally dose a single insulin injection, a patient must use a lancing needle to extract a droplet of blood, prepare a glucometer and place the sample on a test strip for determining their blood glucose as well as estimating the quantity of carbohydrate to be consumed. Then they must calculate how much insulin they require for the planned carbohydrate load, corrected for their present glucose level, and then perform self-injection (10) (see Fig. 1a for the entire workflow). A patient may need to perform these painful procedures and complicated calculations three or more times daily.

A variety of technologies have been developed to help patients with glycemic control, preventing complications, and improving the quality of life in those living with diabetes. Insulin pumps, for example, automate insulin dose calculations and can deliver insulin both continuously and on demand. Continuous glucose monitoring (CGM) technology has drastically reduced the number of finger sticks required (11) and revolutionized the amount of blood glucose data that can be collected (12,13). More recently, hybrid devices, also known as artificial pancreases, have been approved that both monitor glucose and deliver insulin automatically (14,15). However, these devices are expensive, require extensive patient training, have to be worn continuously, and are only accessible to a small percentage of patients, generally with type 1 diabetes (16). Insulin pens, which are simpler, more accurate and patient-preferred over vial and syringe, are in broad use in both type 1 and type 2 diabetes (17). New "smart" pens can wirelessly communicate with a CGM device to acquire blood glucose information and automatically calculate required insulin doses for blood glucose correction (18). However, a need remains for more complete integration of the processes of measuring blood glucose, and estimating carbohydrate consumption – the required information for accurate insulin dose calculation – with insulin delivery. Ideally this system would exist as an easy-to-use device, for the millions of people using insulin and for whom an integrated CGM/pump device is not an option.

We have developed "all-in-one" technologies to facilitate the processes of carbohydrate counting, blood glucose measurement, insulin dose calculations, and insulin self-injections required for routine diabetes management (Fig. 1b-d). An automated carbohydrate counting application utilizing computer vision and food weight estimation with a mobile smartphone has been created to communicate with our two new insulin delivery technologies (Fig. 1b). The first device seamlessly integrates a vacuum-assisted lancing device, a glucometer with test strip, and an insulin delivery pump into a single system. This integrated system automates blood sampling, glucose measurement, and insulin delivery (Fig. 1c) and is fully compatible with commercially available lancets, testing strips, and insulin needles allowing for rapid clinical translation. The second device uses advances in flexible electronics to incorporate a glucose sensor onto the insulin delivery needle and enables glucose sensing in interstitial fluid, dose calculation based on glucose result, and insulin delivery, which fundamentally removes the requirement for separate penetrations of the skin for blood collection and insulin delivery (Fig. 1d). We assessed the insulin delivery workflow for both devices and show that our automated approaches can significantly reduce time burden for the patient and, consequently, our system has the potential to improve the medication adherence, optimal glycemic control and be transformative for diabetes management.

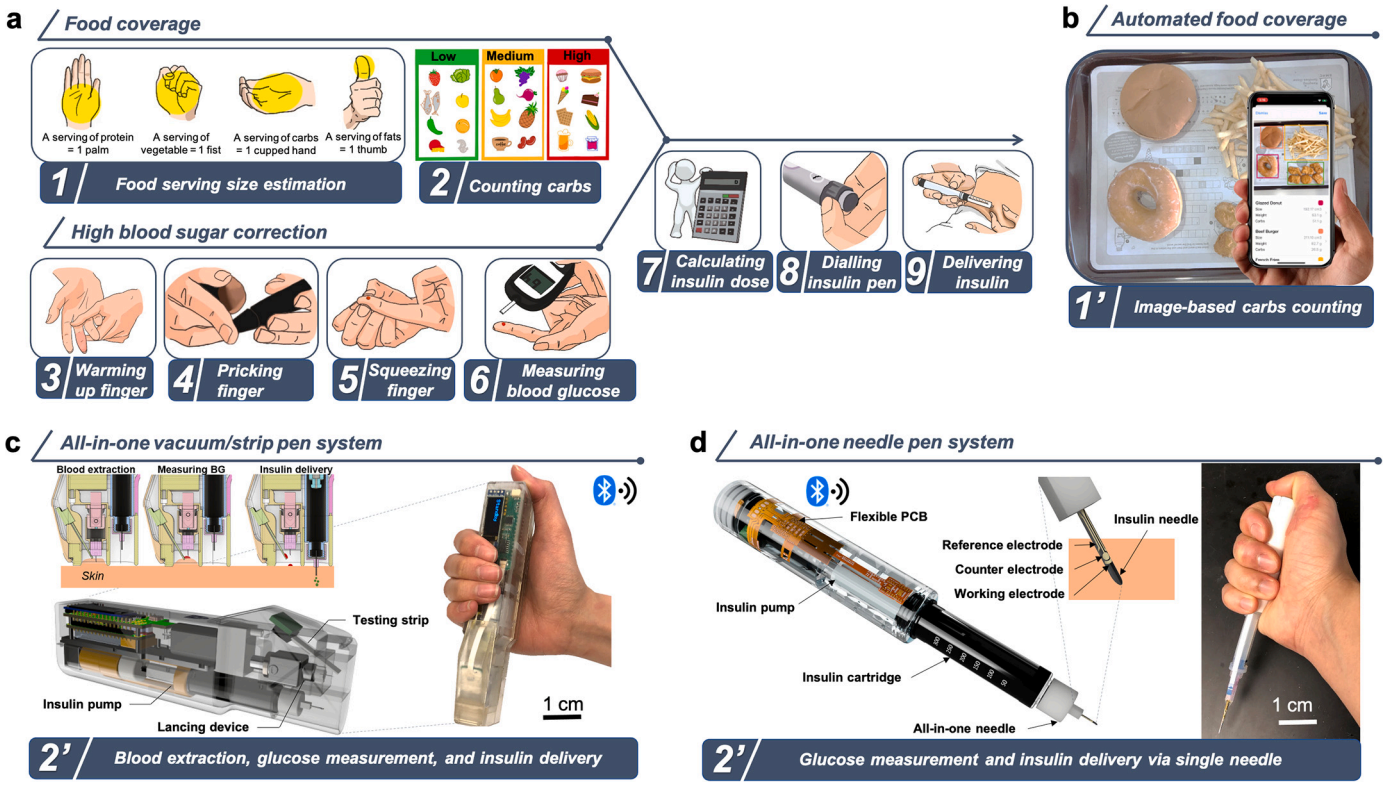

Fig. 1. Pre-prandial insulin delivery. (a) Standard procedures to inject insulin with a safe dose based on food coverage and high blood sugar correction. 1) Estimating food serving size of an intaking meal; 2) counting the total carbohydrate content in the meal; 3) warming up the finger to facilitate blood drop extraction; 4) pricking the fingertip by means of a lancing device; 5) squeezing the finger to obtain a drop of blood, roughly 1 uL; 6) feeding the blood to a testing strip connected to a glucometer and measure the current blood glucose level; 7) calculating the insulin dose based on the blood glucose measurement and carbohydrate estimation; 8) carefully dialing the insulin pen based on the insulin calculation result; 9) subcutaneous injection of insulin. (b) The proposed image-based food carbohydrate estimation system for automating carbohydrate counting. The acquired carbohydrate information was shared to the developed all-in-one insulin pen systems via Bluetooth. (c) The all-in-one vacuum/strip pen system consisted of a lancing device, a blood glucose meter, and an insulin pump, enabling autonomous blood glucose measurement and prandial insulin delivery. (d) All-in-one needle pen system with the same size as a commercially available insulin pen was able to measure body glucose level and deliver insulin through the same needle injection.

2. Materials and methods

2.1. Food carbohydrate estimation

2.1.1. Food data capturing

Food information was captured by taking a single top view image of the foods via a structured light-based depth camera system also known as TrueDepth camera. The raw image data were obtained via our client phone application running on an iPhone X. The captured images by the TrueDepth camera consisted of a color image and a depth map with the same resolution as the color image as well as the camera calibration information including the focal length, the optical center and distortion center coordinate, and the lens distortion lookup table.

2.1.2. Food image segmentation

The segmentation of the food image gave binary labels, food/non-food, for each pixel, and generates a segmentation mask for the colored image. In the mask, pixels for different food objects were assigned to different labels by applying a connected component labeling algorithm. A binary semantic segmentation task that provided food/non-food labels for each pixel was considered first. To generate the binary segmentation mask, U-Net is used with Inception-ResNet-v2 as feature extractor. The model was trained on the Food201-MultiLabel dataset with 9672 images for training and 2418 images for testing, and all kinds of food labels were considered as "food" label. With its feature extractor pre-trained on ImageNet Large Scale Visual Recognition Challenge (ILSVRC) and kept frozen during the training, the model was trained with Lovasz-Softmax loss function and Adam optimizer with an initial learning rate of 10^{-3} for 6 epochs, and 10^{-4} for another 6 epochs. The binary segmentation mask provided by the model was then processed to obtain the multi-label segmentation mask. Activated regions smaller than a certain threshold were removed in order to reduce noise, and a connect component recognition algorithm is used to assign pixels of different food objects with different labels.

2.1.3. Food size estimation

The pixels of the depth map were projected to the 3D space. Specifically, for a pixel in the depth map with the coordinate (x_p, y_p), given the optical center(x_0, y_0), the focal length f, and the pixel's corresponding depth value d, its coordinate in the 3D space was given as:

$$\left(\frac{(x_p - x_o)d}{f} \quad \frac{(y_p - y_o)d}{f} \quad d\right) \tag{1}$$

The geometric position of the background's flat surface, for instance a table, is estimated using the Random sample consensus Random sample consensus (RANSAC) algorithm which gets applied on the generated point cloud. Afterwards, the point cloud was rotated such that the table surface is placed parallel to the XOY surface, compensating slight inclination introduced during the capture of the image. Then, by considering the obtained segmentation mask, we extracted the points of each food object, projected them to the table surface, and split the projected region into grids of 2 mm × 2 mm. The volume of the food was then calculated by the summation of all products of the grid area and the z-axis average distance between the point and the table surface in each grid.

2.1.4. Food classification and carbohydrate estimation

Since Calorie Mama is only able to process one food item at a time, we split the image into multiple sub-images. Therefore, the captured image was cropped and split into individual images each including only one food and further processed individually using the API. As a result, each sub-image was analyzed and the food information including food types and carbohydrate content was extracted. The sub-images were defined by the segmentation mask. Therefore, a square of minimal size with fixed padding covering the food object was used to cut out the food object from the original image. Since the carbohydrate unit from the API was based on weight instead of volume, we developed our own food density library to map food volume to weight. A data collection application was developed to collect food density data from volunteers. The volunteers captured an image of their meal following the image capture requirements, labeled the image with the food name and its weight. The collected data were then manually post-processed to build the density library. Finally, given a food object with volume v, density d, and unit carbohydrate weight c, its carbohydrate weight was calculated as product of v, d, and c.

2.1.5. Food density library

To build the food density library for converting the estimated food volume into food weight, we utilized an electronic balance to obtain the real food weight and divided the food weight by the estimated food volume. Three portions of each kind of foods were measured to get the average food density and the standard deviation (Supplementary Table S1). The density of each food was described as $d = \sum_{i=1}^{N} \frac{W_i}{v_i}$, where W_i was the measured weight by means of an electronic balance and v_i was the estimated volume using our system. The code for implementing the food volume/weight estimation as well as food carbohydrate estimation is available on GitHub (19).

2.1.6. Conventional carbohydrate counting analyses

We enrolled five volunteers with type 2 diabetes to perform the carbohydrate counting study by means of the conventional approach. Nine different types of foods were given to the volunteers to estimate the volume, weight, and carbohydrate content, during which the time was recorded. A nutrient table composed of carbohydrate ratio of the given food was provided. The time was captured until the estimation reached a similar accuracy to the computer vision-based approach.

2.2. Vacuum-based all-in-one insulin pen

All 3D CAD designs were conducted by Autodesk Fusion 360. The cases, actuator holders, and moving objects were made out of clear and durable materials which were directly printed either through Formlabs or Stratasys 3D printer. Circuit designs were conducted by AutoCAD Eagle. The printed circuit board was fabricated by SUNSTONE circuit, USA. The glucose testing strips from OneTouch, insulin needles (32 G, 4 mm) from MedtFine, 18 G lancets from CareTouch were all commercially available products.

2.2.1. Vacuum level control

The lancing device and testing strip were both placed inside the vacuum chamber with cables wiring out to the microcontroller. A micropump (YIMAKER MPA2001S, DC 3 V, 0.23 A) was connected to a N type MOSFET in series to enable the controllable vacuum pressure. Pulse-width modulation was used to vary the gate to source voltage of the MOSFET from 0 V to 5 V, thus changing the vacuum from 15 PSI to 5 PSI (Supplementary Fig. 5). The vacuum environment was achieved when the open side was touching the skin to form a sealed condition. The pressure in the vacuum chamber was measured by a pressure sensor (MPRLS, Honeywell) with the range from 0 to 25 PSI.

2.2.2. Blood glucose meter

A blood glucose meter based on integrated chip potentiostat (TI LMP91000) was developed to measure the blood glucose level by means of a commercial testing strip. The circuit design is provided in the supplementary information. Cyclic voltammetry (CV) was first applied onto the commercial testing strip with the bias voltage scanning from −800 mV to 800 mV (Supplementary Fig. 4a). The oxidation peak was observed to be 150 mV. Amperometric detection is used to measure the glucose level with the bias voltage of 150 mV. Testing of our glucose meter using commercial test strips indicated it has comparable

performance a commercial glucometer (Supplementary Fig. 4c). The output current flow into the working electrode was then amplified by a transimpedance and a non-inverting operational amplifier. The amplified signal is then fed into an analog to digital converter. A commercially available glucose meter (One Touch Ultra 2) was used to verify and calibrate the blood glucose reading.

2.2.3. Lancing device, insulin pump and needle injection

The lancing device is driven by a micro-DC geared motor with diameter of 6 mm and length of 19 mm (5 V, 30 mA, 500 RPM, stall toque of 500 g-cm) to provide the system with a high lancing speed and strong enough skin penetration force. The 3D-printed lancing driver converts the unidirectional rotation from the motor to a bi-directional linear movement. A ring-shaped magnet (R1013D, SUPERMAGNETMEN) magnetized across diameter was attached on the lancing driver to provide positioning feedback. A hall-effect sensor (US5881lUA) was placed next to the magnet capturing the changes of magnetic field to enable closed-loop control of the lancet actuation. The insulin pump is composed of an insulin needle, syringe-like insulin cartridge, screw plunger, and two phase four wirers geared stepper motor with lead screw. The insulin pump was directly connected to and driven by a micro DC geared motor (3 V, 30 mA, 100 RPM) for controlled needle injection. A square magnet (S0510D, SUPERMAGNETMEN) magnetized through width was embedded in the injection motor driver for positioning feedback. A hall-sensor was also placed next to the square magnet to capture the changes of magnetic field induced by the injection motor, thus enabling the closed-loop control of the automatic insulin needle injection. The insulin cartridge, screw plunger, and the stepper motor holder were 3D printed with Formlabs using durable materials. Pumping rate was controlled by the speed of changing steps through a driver. The insulin cartridge was pre-filled from commercially available insulin vials using a syringe. The cartridge was then loaded in the insulin pump before use. The DC motor was equipped with a hall sensor as an encoder giving feedback position information of the insulin pump in which a magnet was attached. An H-bridge circuit was employed to control the velocity and direction of the DC motor.

2.3. Microfabrication of glucose sensing electrodes

2.3.1. Polydimethylsiloxane (PDMS) layer

A 3″ silicon oxide wafer (Nova Materials, CP02–11208-OX) was silanized in a vacuum chamber under vacuum in the presence of a drop of 1H,1H,2H,2H- Perfluorooctyltrichlorosilane (Silane, Oakwood Chemical, 78,560–45-9) for 20 min. Subsequently, the silane bonding was finalized with a hotplate bake at 120 °C for a minimum of 3 min and the silanized wafer was thoroughly cleaned using acetone and IPA. SYLGARD 184 silicone (Dow-Corning) was prepared by mixing base with curing agent at a ratio of 10:1 and spin-coated onto the prepared wafer at 500 RPM for 5 s followed by 4000 RPM for 45 s. The resulting wafer was baked in an oven at 65 °C for at least 12 h.

2.3.2. Bottom polyimde layer

Polyimide solution was prepared by mixing VTEC PI-1388 with 1-methyl-2-pyrrolidinone (Sigma-Aldrich, 443,778) at a ratio of 2:1 at room temperature using a Speedmixer. The PDMS coated wafer was subjected to an O2 plasma (100 W, 50 sccm, 30 s) surface treatment, followed by spin coating of the prepared PI solution at 4000 RPM for 45 s. The wafer was then soft-baked at 65 °C for 4 min before gradually headed to 200 °C for a 2 h hard bake, followed by allowing to cool to room temperature gradually to avoid film cracking due to temperature shock.

2.3.3. Electrode layer

For electrodes designed for the 18G needles a laser cut patterned Kapton shadow mask (McMaster-Carr, 2271 K3) was used. For electrodes designed for 25 G needles, a photoresist mask of LOR3A spincoated at 4000 rpm, and baked at 115 °C for 4 mins, followed by S1805 spincoated at 4000 rpm, and baked at 115 °C for 4 mins, was coated onto the wafer and then exposed to the designed pattern using a Heidelberg MLA150 maskless aligner. In both cases, the wafer was then loaded into an electron beam evaporator where 5 nm of Ti followed by 100 nm of Au was deposited. The photoresist coated wafers then underwent liftoff processing in acetone for ca. 4 h.

2.3.4. Top polyimide layer

The top passivation layer was prepared as described previously [2].

2.3.5. Reactive ion etching of Polyimide

An etch mask was fabricated in one of two possible methods: (a) S1822 was spincoated into the wafer at 3000 RPM for 45 s and baked at 115 °C for 3 min. Etch windows were exposed using photolithography as described in reference [3]. (b) Deposition of Ni using a laser cut kapton shadow mask. Etching of polyimide to expose electrochemistry electrodes and input/output pads was done using reactive ion etching in a gas ratio of 5:2 O2:CF4. Following etching, the S1822 etch mask was removed in acetone while the Ni etch mask was removed in TFB Nickel etchant (Transene Co. Inc).

2.4. Glucose sensing modification preparation

A 30 mg/mL Hexaamine Rutheniumn (Sigma) in Chitosan (0.5% in 1% acetic acid) solution was prepared by stirring at 300 rpm and heating at 80 °C for 4 h. 4 uL of NaOH (2 M), 5 uL of glucose oxidase (Gox) in water (50 mg/mL) and 10 uL of Glutaraldehyde (1% in water) were added to 100 uL of the HexaRu solution. Three layers consisting of 2 uL each were deposited on the working electrode while waiting 30 min for each layer to dry. Subsequently a 1.5 uL layer of Nafion (0.5% in water) was drop cast and left to dry for 30 min.

2.5. All-in-one needle assembly

2.5.1. Release of electrodes from silicon wafer

Water soluble transfer tape (SmartSolve, OH, USA) was applied to the surface of the microfabricated electrodes on the silicon wafer. The silicon wafer was then cut using a diamond scribe, on the back face, which enabled peeling of the electrodes/transfer tape from the wafer. The resulting electrodes were cut into a rectangular shape and the target needle and the exposed PDMS face was treated with corona plasma.

2.5.2. Wrapping of electrodes

A commercial luer-lock needle with a 3D printed needle hub was coated with silicone, and exposed to corona plasma treatment to facilitate electrode bonding. The cut electrode films were floated on the surface of water until the water-soluble transfer tape was dissolved, and the needle was aligned with the electrode pattern and transferred. The completed needle electrodes were baked in a vacuum oven at 80 °C to ensure tight bonding of the silicone layers in manner similar to the reported in literature.

2.5.3. Reference electrode preparation

Ag/AgCl paste (Creative Materials, 117–23) was applied to the reference electrode using a pipette and annealed at 100 °C for 1 h.

2.5.4. Working electrode preparation

Three microliters of the prepared modification solution was drop cast onto the center of the working electrode and then allowed to dry. Then 3 uL of 0.5% Nafion solution was drop cast on top of the working electrode to provide a water/glucose permeable encapsulation of the modification.

2.5.5. Electrical connections

Electrical connections were made using a layer of anisotropic

conducting tape (3 M 9703) followed by connection to Premo-flex cable (Molex, USA), into either a custom potentiostat circuit or a DY2000 (Digi-IVY, INC) potentiostat.

2.6. Animal testing of all-in-one systems

All in vivo studies were approved by the Massachusetts Institute of Technology Committee on Animal Care. Female Yorkshire swine (Tufts, Medford USA) in the range of 60–80 kg were used for the testing of all-in-one needle and all-in-one vacuum/strip pen systems. The animals were kept on a liquid diet for 24 h before the procedure and fasted overnight. Pigs were sedated with intramuscular injection of Telazol (2-6 mg/kg) and Xylazine (2–4 mg/kg) and were kept on isoflurane (1–2%) and oxygen (2–3%) either via a face mask or endotracheal tube. For blood sampling, an indwelling catheter (Central venous catheter kit, 7Fr-30CM (12″), JORGENSEN LABS INC.) was placed in the femoral vein under asceptic conditions. Blood glucose levels were measured by TRUEtrack Blood Glucose Test Strips and TRUEtrack glucometer.

Blood extraction using the Genteel vacuum-assisted lancing device and the all-in-one vacuum/strip system was performed on the porcine ears. Four ears were uniformly lanced 20 times in each condition; as a result, four different pigs were lanced 80 times in total. The success of blood extraction and the volume of extracted blood were recorded subsequently. The lancets of both the Genteel device and the all-in-one system were replaced every three times to maintain the sharpness. The automated insulin injection was also performed on pig ears by means of a 34 G needle.

Measurements using the all-in-one needle were conducted by inserting the needle into the thigh of the animal following use of a 16 g introducer needle. To prevent hypoglycemia during anesthesia, blood sugar level was maintained by delivery of a bolus of 10 mL of 50% dextrose solution (VEDCO Inc.) when measured blood glucose was observed to fall below 20 mg/dL.

3. Results and discussion

3.1. Food carbohydrate estimation

Carbohydrate counting is an established approach used by patients with diabetes treated with insulin, as it enables greater precision in insulin dosing and improves glycemic control (8,20,21). However, this requires accurate estimation of portion size as well as understanding of the nutrient information per weight of the food, in order to calculate the carbohydrate content of each individual food, and then adequately calculate the indicated bolus insulin dose (22). This process is notoriously difficult and fraught with human error, and estimation errors can result in over- or under-dosing and therefore impact both the safety and efficacy of an insulin dose. In the past decade, researchers have investigated various computer vision-based approaches to help patients with approximating food portion size, classifying food types, and estimating nutrient contents. Existing systems, such as GoCARB (23,24), use stereoscopic vision to capture at least two images at different angles for 3D geometry reconstruction. To estimate the food volume, stereoscopic vision requires an additional reference object placed next to the meal to serve as a scale bar. A major drawback of using a stereo camera is thatthe 3D models cannot be reconstructed and the volume estimation will fail if the food surface does not have distinctive characteristics or texture (25). Moreover, the accuracy of volume estimation could be easily affected by changes of ambient lighting conditions (26). To address the suboptimal volume reconstruction using the stereoscopic vision, here, we employed a structured light-based depth camera that does not require a reference object during capturing, requires a single image, and has higher accuracy in 3D geometry reconstruction to mitigate the effect of food texture and ambient lighting conditions.

Fig. 2(a) outlines the following procedures after taking the food image via the structured light-based depth camera (see Supplementary Note 1 for the guidance on using TrueDepth camera for estimating food volume). The colored image is used to generate a food segmentation mask that recognizes food objects. The segmentation algorithm recognizes that there are different foods on each plate individually and marks them with distinct labels. The segmentation mask together with the depth map enables the generation of the food point cloud; the depth map and camera calibration data are used to obtain the base plane of the 3D point cloud. By subtracting the food point cloud with the base plane and then projecting it to the x-y plane, we obtained the food histograms of each individual food. Subsequently, the food volume is obtained by integration of the food histogram. Food weight estimation based on the measured food volume can be calculated using a self-generated food density library (Supplementary Fig. 1). To identify the food types and obtain the nutrient library of each food, we employed a commercial API called CalorieMama (27). Using this workflow automated by our mobile application, our system is able to recognize multiple types of food simultaneously from a single top view image. For example, four different kinds of fast food including beef burgers, chicken nuggets, french fries from McDonald's, and a glazed donut from Dunkin' Donuts, all with diverse spatial geometries, can be simultaneously identified. With the estimated food weight from our model and the carbohydrate information about each type of food from the commercial API, individual food carbohydrate content for the photographed portion size can be estimated. In addition, Supplementary Movie 1 shows that our method is able to recognize two different kinds of unfinished donuts on the same plate and accurately estimate their volume, weight, and carbohydrate content.

Although our system can estimate food carbohydrate content through a single top view image, the accuracy depends on the input image quality. Any perturbation during the operation will have the potential to induce deviations in the volume prediction. To test the robustness of our system, we first defined two common positioning variations, height and central offset, and two orienting variations, pitch and roll angle. Supplementary Fig. 2 show the characterization of the defined operational variations versus the error in the estimation of food weight. The estimated food volume and weight are also provided in Supplementary Fig. 2. The relative food weight estimation errors, defined as $\frac{estimated\ weight - measured\ weight}{measured\ weight}$, in the food weight estimation are all within 10%. The distance between the food object and the camera was varied from 35 cm to 50 cm resulting in an error in weight estimation at below 5% (Supplementary Fig. 2e-2h). The central offset is defined as the horizontal distance of the food object away from the center of the camera view along the diagonal direction. Central offsets of up to 10 cm were characterized (Supplementary Fig. 2f). The French fries were outside of the camera's field of view when the central offset was larger than 6 cm as the volume of French fries is significantly larger than the other foods (Supplementary Fig. 3b). The orienting variations of the pitch and roll are ranging between −30 and 30 degrees. The pitch and roll variation also induced changes in height ranging from 5 to 15 cm due to the asymmetric placement of the camera on the body of a smartphone, possibly explaining the larger observed errors (Supplementary Fig. 3c and d). For instance, it causes the camera height to decrease when the pitch angle is positive, while a negative pitch angle leads to an increase in a camera height.

To further validate the accuracy of our carbohydrate estimation system, we tested it with a variety of other cuisines including fried rice, soba, nigiri, Bibimbop, spaghetti, and salmon steak as well as fruit with both high and low carbohydrate content, such as a banana, pineapple, and avocado. Fig. 2(b) shows the segmentation masks accurately outline the foods from the dishes and the food histograms precisely capture the depth of the segmented foods. Fig. 2(c) and 2(d) show the averaging weight and carbohydrate estimation of each food versus the ground truth results with the corresponding mean errors (see the root mean squared errors in Supplementary table I). The ground truth weights of each food were measured via a scale. The ground truth carbohydrate

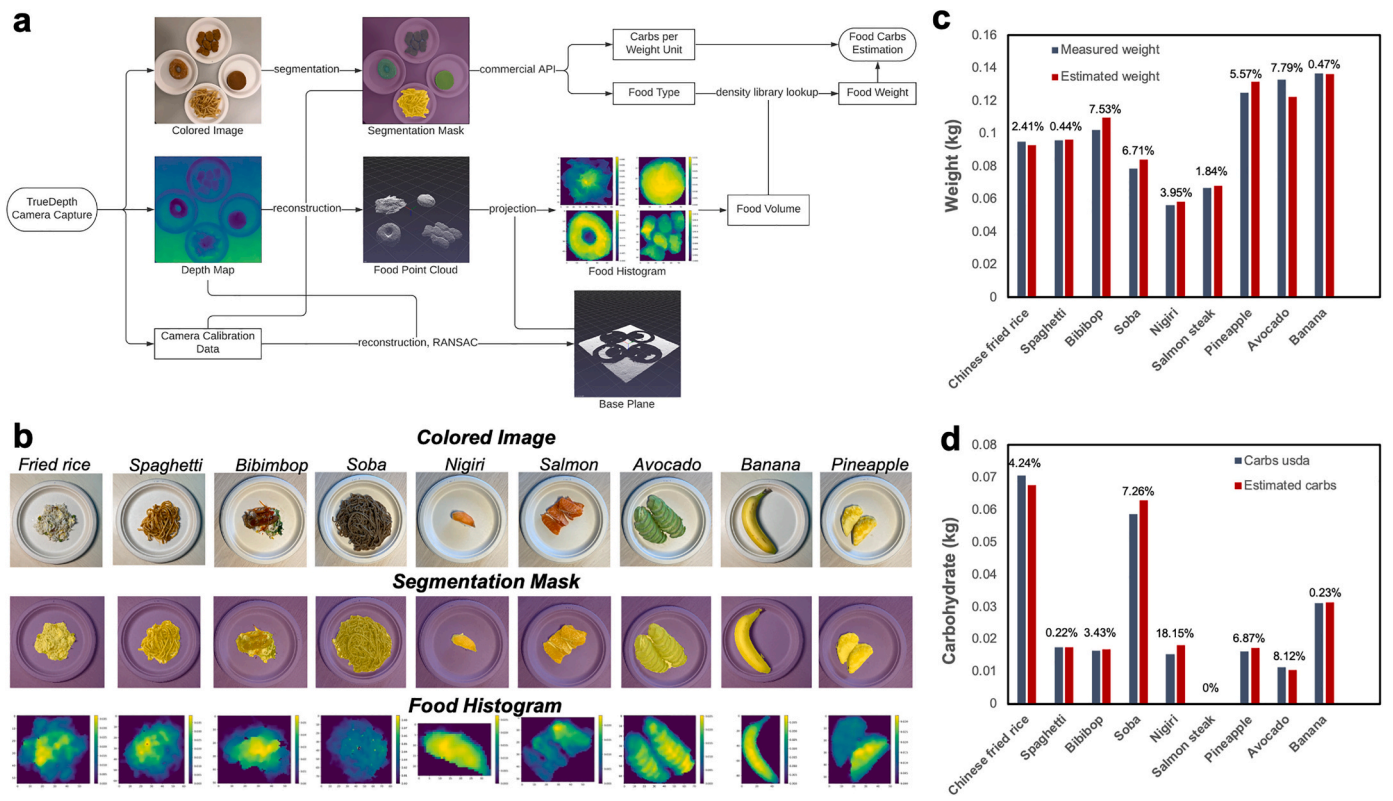

Fig. 2. Food carbohydrate estimation system. (a) Flowchart of estimating food carbohydrate contents using a TrueDepth camera. (b) Validation of the food segmentation and food histogram for volume estimation using the colored image and depth map. Scale bar 50 mm. (c) Estimated food weights versus the scale-measured food weights. (d) Estimated carbohydrate based on the estimated food weight and the nutrient information from Calorie Mama versus the ground truth results based on the scale-measured weight and the nutrient information from USDA. The food weight and carbohydrate were measured with $n = 3$ of separate dishes for each type of food.

content was obtained by multiplying the measured food weight with the carbohydrate units provided by the United States Department of Agriculture (USDA). Our estimation results show good consistency with the ground truth results for most foods, except that of nigiri with a mean error of 18.5%, while the mean error of the weight estimation is only 3.95%. Therefore, it is clear that the error source is from the discrepancy of food nutrient dataset between Calorie Mama and USDA (see Supplementary table I). Therefore, it is suggested that a unified nutrient library is in need to address the data source discrepancy to enable more reliable carbohydrate counting using either manual approximation by the user or computer vision-based estimation.

In addition, we observed that the documented carbohydrates of most fast foods are measured based on the portion size; however, the actual weight of each portion served may vary significantly (28). For instance, the officially labeled carbohydrate content of medium-sized McDonalds' French fries is 25% lower than our estimated result, while the actual weight is within the error of our estimated weight using our system (Supplementary Fig. 2i and j). If a person counts carbohydrate content based on the provided label, then the person might consume more carbohydrates than expected. In contrast, our system can accurately estimate the actual food weight, and provides the user with a reliable method of carbohydrate counting.

3.2. All-in-one system for blood glucose correction

To determine the insulin dose for pre-prandial delivery, a patient needs to know not only the bolus insulin dose needed based on food ingested, but also the dose correction needed based on current blood glucose levels. Patients measure blood glucose level by pricking their finger using a lancet to extract blood and transfer it into a testing strip. To obtain sufficient blood volume for accurate blood glucose measurement and reduce the finger prick pain, patients usually need to (I) warm their hands to increase blood flow before lancing and (II) squeeze their fingers to expel blood after lancing (See Fig. 1a, step 3 to 5).

Our first all-in-one pen system is designed to automate the procedures of obtaining a blood sample, measuring glucose levels, and delivering the calculated bolus insulin via a single device. This system seamlessly integrates a motorized lancing device, glucose meter, vacuum chamber, injection motor, and insulin pump (Fig. 3a). The user first manually loads a commercial testing strip, lancet, and insulin needle (see Supplementary Movie 2). The pen system is initiated by the developed iOS mobile application. After the pen receives the carbohydrate estimation results, the user then will have five seconds, a self-defined period, to place the device at the desired injection site. After device placement, the system will initiate a vacuum to induce skin stretching and hold the vacuum for five seconds to induce a local increase of blood flow and an analgesic effect (29,30). Then, a motorized lancing device will be actuated to prick the skin (See Fig. 1c and Supplementary Movie 2). After lancing, the vacuum will maintain for another five seconds, and then allowed to return to atmospheric pressure. The generated pressure gradient between the stretched skin and the chamber will then drive the blood sample extraction. After five seconds remaining at atmospheric pressure, a final vacuum with the same amplitude will be applied again to stretch the skin to feed the blood drop into the testing strip. The onboard glucose meter measures the blood glucose level and converts it into the required insulin dose. Full characterization of the onboard glucose meter is shown in Supplementary Fig. 4. The injection motor is subsequently actuated to administer the calculated insulin dose via a subcutaneous injection (see Supplementary Movie 3 for the fully automated procedures). The delivered insulin dose, the measured blood glucose, and the intake carbohydrate

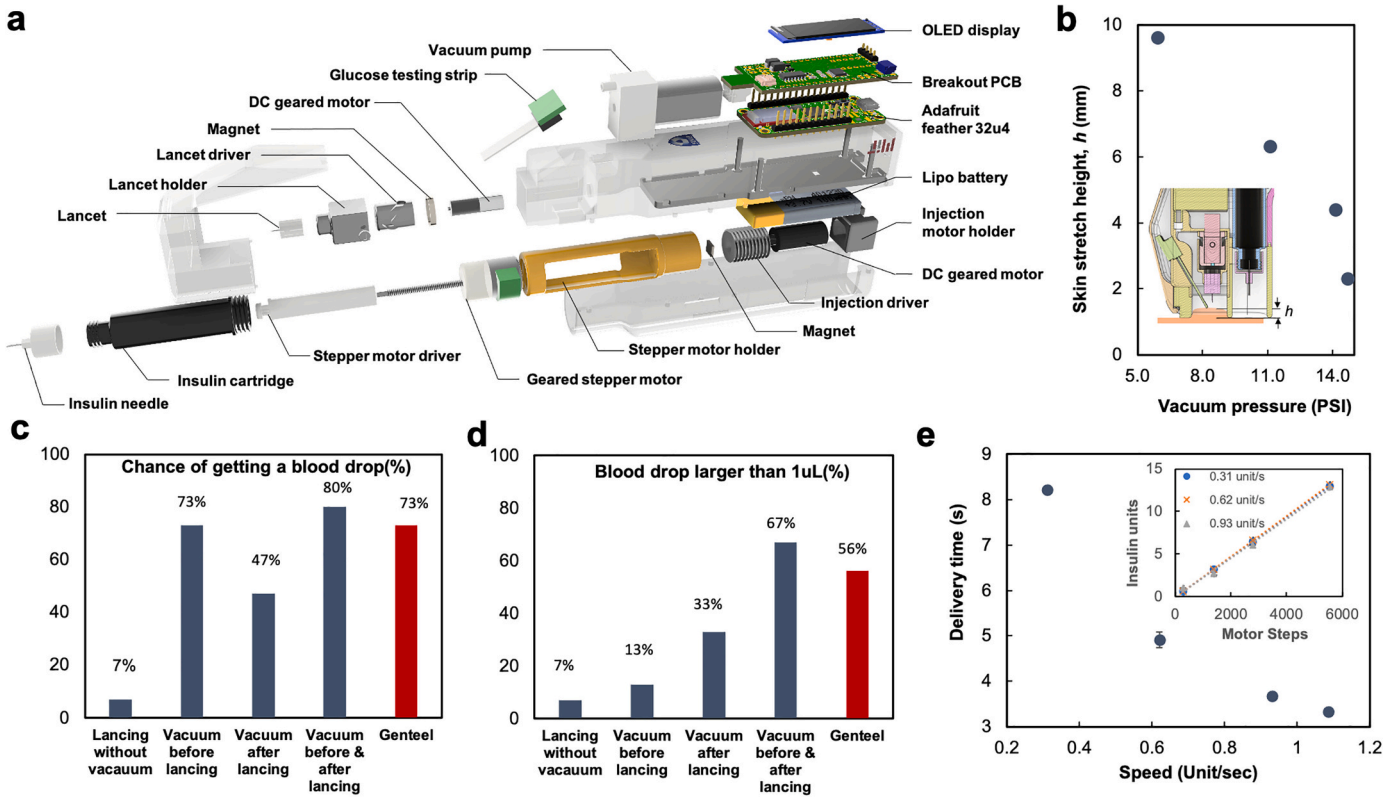

Fig. 3. Design and characterization of the all-in-one vacuum/strip pen system. (a) Exploded view of the all-in-one vacuum/strip pen system. (b) Vacuum effect on skin stretching, performed on swine ears. (c) Chances of getting blood drops at various conditions. The skin stretching height were measured with n = 3 from separate pig skins. (d) Chances of getting a blood drop that was larger than 1 uL at various conditions. The chances were obtained by performing each condition 20 times among four different swine. (e) Required time for pumping 3 units of insulin in three different swine thighs at various speeds.

content are automatically recorded on the developed mobile application.

3.3. Vacuum effect on blood extraction

To enable automated blood extraction for blood glucose testing, we introduce a vacuum system to induce skin stretching and blood draw before and after lancing respectively. This resembles the actions of warming up the hands to increase blood flow and squeezing the finger to accumulate and extract blood in a local region. The stretched skin height is proportional to both the cross-section area of the open channel and the vacuum pressure (29). Here, we controlled the vacuum pressure to modulate the skin stretching height with a fixed cross-sectional area of 2 cm^2 as shown in Fig. 3b and Supplementary Fig. 5. The results were obtained from porcine ears as it is the area with the most similar mechanical properties to human skin (31). The stretching height determines the position of the lancet device, resulting in different lancing depths. We positioned the lancet device based on the vacuum pressure of 5.5 PSI to keep a constant lancing depth and maximum skin stretch height. To verify the vacuum effect on blood extraction, we made a comparison between four different conditions that are (I) lancing without vacuum, (II) vacuum only before lancing, (III) vacuum only after lancing, and (IV) vacuum before and after lancing. Fig. 3c shows the probability of blood extraction in the four conditions. We observed that applying vacuum can significantly increase the chance of successful blood extraction. Moreover, applying vacuum before lancing resulted in a much higher chance (73%) of a successful blood draw compared to vacuum application after lancing (47%). This observation suggests that the skin stretching before lancing is necessary as it approximates the action of local heating to induce increased blood flow. However, we observed that applying vacuum only before lancing does not result in sufficient blood for glucose measurement (Fig. 3d). To obtain an accurate glucose reading, commercial test strips require more than 1 uL of blood (32). We observed that applying vacuum before and after lancing has a significantly higher chance of getting a blood drop with a volume larger than 1 uL than that only applying vacuum before lancing. As a reference to the success rate of blood extraction from the porcine ears, we employed Genteel (33), an FDA approved painless lancing device that also utilizes vacuum to assist blood extraction, to evaluate our system. It is worth noting that a hot pack and hand-squeezing are used together to warm up the porcine ears before lancing with the Genteel device. Without these procedures, it is impossible to extract blood from the porcine ears by means of the Genteel device. Thereby, our system shows an equivalent performance as the commercial Genteel device without performing the additional heating procedures.

3.4. Insulin delivery

Having obtained the food carbohydrate content and the blood glucose reading, the all-in-one pen calculates and delivers a bolus insulin dose. A bolus calculator (34) is encoded both in the all-in-one insulin pen system and the smart phone application. The calculator encoded in the all-in-one pen system is responsible for high blood sugar correction based on the blood glucose measurement while the calculation on the smart phone Application is responsible for the carbohydrate correction based on the carbohydrate intake estimation. The users have to manually input the insulin sensitivity factor and the insulin-to-carbohydrate ratio obtained from their doctor into the smart phone as an initialization setting. To confirm accurate dose delivery, we tested our insulin pump by varying the number of insulin units delivered and the speed via in vitro injection into air. The inner figure in Fig. 3e shows that delivered insulin units were linearly proportional to the controlled motor steps

and there is no difference in the accuracy (±2%) of insulin delivery between various speeds. The required delivery time dramatically dropped as we increased the flow speed. Supplementary Fig. 6a also shows that the pumping time is linearly proportional to the required insulin units. Standard guidelines for usage of a commercial insulin pen require holding the pen for more than 10 s after fully dispensing the insulin to ensure residual drops in the pen are delivered (35,36). Similar to commercial insulin pens, we observed residual drops with volume of less than one unit of insulin, independent of pump speed (Supplementary Fig. 6b). However, we observed that there was no increase in residual drop size between 5 and 10 s after stopping the insulin pump, suggesting that this "hold time" could be decreased, to improve ease of use of our system compared to the current standard of care. In sum, the all-in-one vacuum/strip pen system automates the steps of pre-prandial insulin delivery using commercially available components, which mitigates potential risks and enhances the success of clinical translation.

3.5. All-in-one needle

Following our development and characterization of the all-in-one vacuum/strip pen system, we set out to develop an all-in-one insulin needle/pen system consolidating separate diabetes management devices into one complete package. Specifically, we aimed to (I) reduce the size of the all-in-one device to a size comparable to a conventional insulin pen and (II) further improve the ease and time of use using new technologies. To this end, we identified that it would be necessary to move beyond the current paradigm based on the standard of care using a separate lancet, testing strip, and insulin needle, which results in a bulky device and increases patient discomfort from the requirement of puncturing their skin through multiple separate needles (37). Motivated by recent developments in surface-conformal flexible electronics (38–41), we aimed to recapitulate the functionality of a glucose sensing strip directly affixed onto the surface of an "all-in-one" insulin delivery needle (Fig. 4a). In contrast to existing glucose sensor implants such as the FreeStyle Libre (42) or Dexcom G6 (43), we envision the glucose sensing capability to be incorporated into a disposable, one time use insulin needle. With the all-in-one needle, the patient's pre-prandial glucose level can be measured immediately following insertion of the needle when the sensor comes into contact with glucose-containing interstitial fluid. The glucose content of interstitial fluid is recognized to be proportional to that of measured blood glucose levels (44). This removes the need to perform separate steps for skin preparation, lancing, vacuum application, and blood draw, which both reduces the number of required device components, and the time for insulin delivery.

To realize this device concept, we first used a scalable microfabrication technique for flexible electronics to manufacture thin film electrodes consisting of a (I) polydimethylsiloxane (PDMS) layer for adhesion/bonding on a silicon wafer, (II) bottom polyimide layer for electrical passivation, (III) metallic electrode layer and (IV) top polyimide layer with exposed windows for electrode input/output (Fig. 4b and Supplementary Fig. 7). We chose these materials for their previously reported biocompatibility when used in bioelectronic implants and sensors (39). We designed the electrode layers to have a set of 3 electrodes including working, counter and reference electrodes in a manner similar to that found in commercial glucose test strips (See Fig. 1d). Following fabrication, these electrodes can be peeled off from the silicon wafer substrate using a water-soluble transfer tape (Fig. 4c, see Methods for details), and transferred/bonded onto the surface of needles with varied gauges (Fig. 4d), where the transfer does not block the channel of the needle. To functionalize the needle for glucose sensing, we coat the

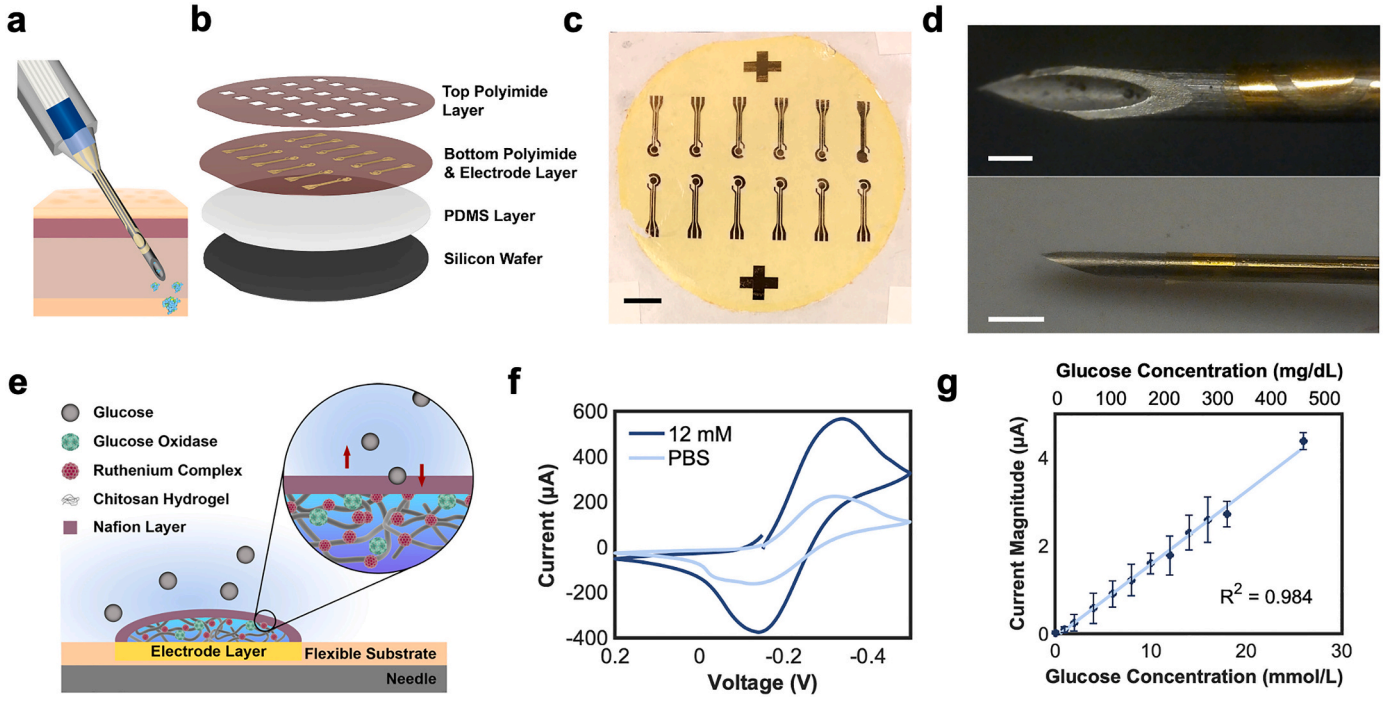

Fig. 4. Fabrication and characterization of the all-in-one needle. (a) Schematic representation of glucose measurement and insulin delivery through a single subcutaneous injection. (b) Schematic representation of fabrication layers of flexible electrodes. (c) Optical image showing array of fabricated flexible electrodes following release from Si wafer carrier substrate using water soluble transfer tape. Scale bar 10 mm. (d) Optical images of flexible electrodes wrapped around commercial 18 G (top, scale bar 1 mm) and 26 G (bottom, scale bar 1 mm) hypodermic needles. (e) Schematic representation of drop-cast glucose sensing modification on working electrode. (f) Cyclic voltammetry results of modified electrodes in 12 mM glucose solution vs. phosphate buffered saline, indicating that the electrodes have been sensitized to the presence of glucose. (g) Measured current during chronoamperometric measurement vs glucose concentration for modified electrodes in vivo highlights the linearity of sensor response up to 26 mmol/L. The working electrode in these measurements was set to 0 V, and current values were taken after running the sensor for 15 s to remove capacitive transients from sensor initialization. Each glucose concentration was measured with n = 3 separately modified electrodes and freshly modified electrodes were used for each glucose concentration.

reference electrode with a drop of Ag/AgCl paste, and the working electrode with a drop of chitosan-ruthenium-glucose oxidase complex followed by a drop of encapsulating Nafion (Fig. 4e, methods). This functionalization results in a second generation type glucose sensor where the ruthenium hexamine acts as an electrochemical mediator (45).

The completed and functionalized electrodes were then connected to a commercial potentiostat. CV performed on the electrodes confirmed the incorporation of the functionalization (Supplementary Fig. 8) and showed the sensitivity of the electrodes to glucose with reduction/oxidation peaks, which corresponded to the values of about −0.1 to −0.2 V given in the literature (Fig. 4f). A key advantage of this modification was that the electrochemical reaction can be monitored at 0 V on the working electrode, and thus we minimized the sensor warm-up time (Supplementary Fig. 9). In addition, electrochemical side reactions are minimized, as evidenced by the minimal cross-sensitivity of our sensor to the approximately 30 interfering substances listed in the FDA guidelines (Supplementary Fig. 10 and Table II) as commonly reported biologically interfering species. We further characterized the performance of our glucose sensing functionalization using chronoamperometry. These measurements showed the current response of our sensor remains linear up to at least 26 mM (468 mg/dL) of glucose in phosphate-buffered saline (Fig. 4g, Supplementary Fig. 11) for a variety of measurement times (5,10,15 s) and provided sufficient dynamic range for expected glucose levels in patients with diabetes. Finally, to alleviate concerns regarding mediator toxicity, we showed that the ruthenium content released by one sensor during transient use (generously estimated to be max of 2 mins) is lower than the daily United States pharmacopeia guidelines and can be further reduced using additional layers of Nafion/chitosan encapsulation which ensures at least four times use during a day (Supplementary Fig. 12).

3.6. In vivo characterization of the all-in-one needle

After verification of our all-in-one insulin needle in vitro, we used our all-in-one needle for chronoamperometric measurement of interstitial glucose levels in a porcine model (Fig. 5a). One representative trace of the chronoamperometric measurement is shown in Fig. 5b. Following needle insertion at $t = 0$, the current magnitude first increased rapidly due to wetting and diffusion of the interstitial fluid into the working electrode and then stabilized within 5–15 s, yielding a stable measurement current which can be calibrated to a known blood glucose level. When the needle was withdrawn from the tissue, there was a sharp spike corresponding to mechanical perturbation, followed by the current amplitude dropping rapidly to the baseline measurement prior to insertion.

A total of 14 measurements were conducted using separate all-in-one needles on different animals with varied blood glucose levels to generate in vivo calibration curves (see Fig. 5b and Supplementary Fig. 13) mean current magnitude in the time windows of 0–5, 5–10, and 10–15 s post insertion vs measured blood glucose. A linear correlation was observed in all 3 time windows, with the 5–10s time window showing highest coefficient of determination (Figure 5biii). This middle time window may yield the best linear response as a balance between giving sufficient time for wetting of the sensor and diffusion of glucose while minimizing depletion of local concentration of glucose from prolonged electrochemical reactions. We attributed the increased variation in our in vivo measurements as a consequence of variability in sensor wetting kinetics, possibly due to needle insertion location/procedure, which influences presence of sufficient amount of interstitial fluid that may affect sensor

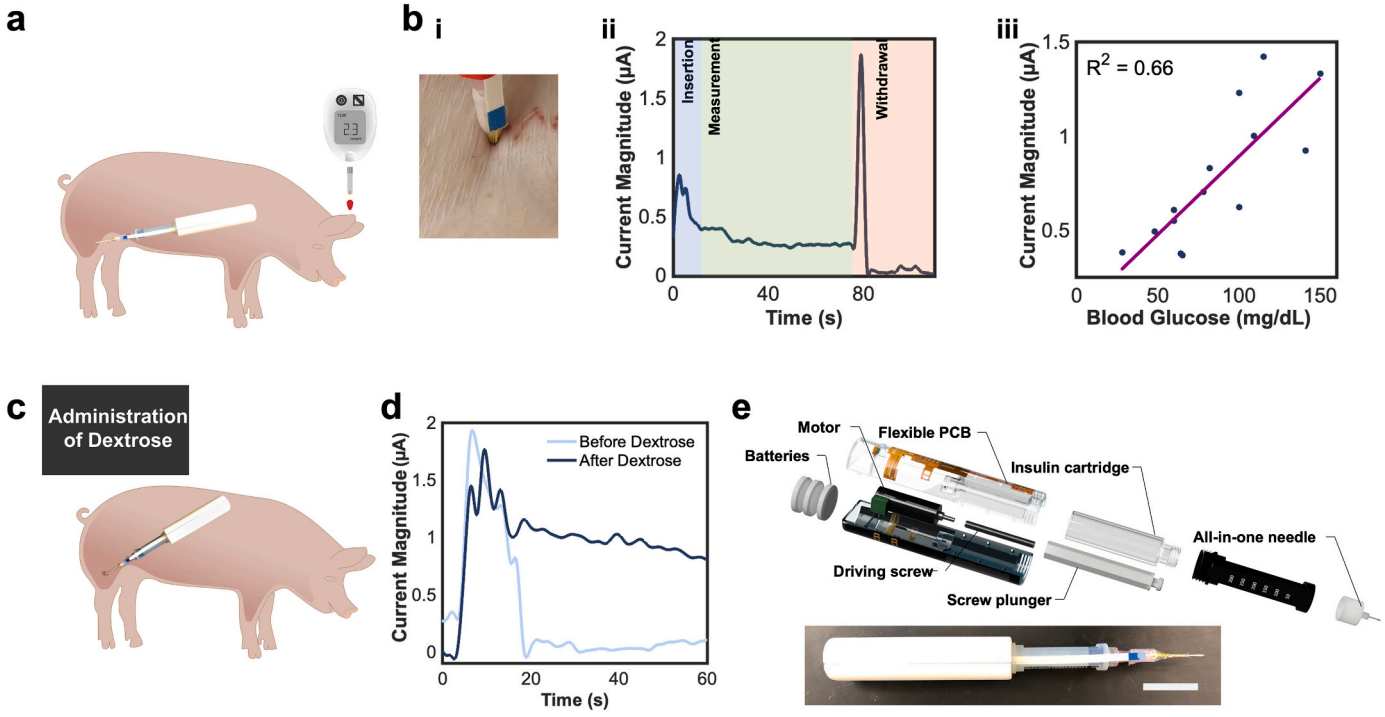

Fig. 5. In vivo characterization of the all-in-one needle. In vivo testing of all-in-one needle sensor in porcine model. (a) Schematic representation measurements comparing all-in-one needle connected to potentiostat in chronoamperometric recording and conventional glucometer with test strip. (b) (i) Optical imaging showing insertion of all-in-one needle into the thigh of porcine model. (ii) Representative current magnitude vs. time plot showing a standard measurement. Needle insertion occurred at time = 0 s, the initial current decreased until stabilization around 10–20s. The upward direction at the end of each recording indicated withdrawal of the needle. (iii) Mean current magnitude between 5–10s post insertion vs. measured blood glucose concentration for $N = 14$ separate animal measurements. (c) Schematic of measurement using all-in-one needle following dextrose delivery. (d) Recording of current vs time recorded using all-in-one needle prior to (BG = 42 mg/dL), and following dextrose injection (BG = 105 mg/dL in a non-diabetic animal where the downward drift during measurement following dextrose delivery is the animal's self-regulation of glucose levels to return to the euglycemic range. (e) Optical image of all-in-one needle with FCC connector into all-in-one pen system. Scale bar 10 mm.

equilibration time. Future work can also potentially improve sensor precision by controlling sensor insertion depth, automating insertion protocol and further standardizing measurement location on a per patient basis.

To further confirm the functionality of our sensors, measurements were conducted using two separate all-in-one needle sensors, prior to and 8 min following the delivery of a 50% dextrose solution via a femoral catheter (Fig. 5c). The delay time between measurements was selected to account for the time delay due to diffusion of glucose from blood into the interstitial fluid, as previously reported (44). The separate recordings (Fig. 5d, Supplementary Fig. 14) in multiple experiments showed an increase in measured current magnitude following dextrose delivery and was corroborated by simultaneous measurements using a commercial glucometer, consistent with a spike in the blood glucose level induced by dextrose injection that resulted in a subsequent increase in interstitial glucose concentration.

Finally, we show that we can incorporate our all-in-one needle into the all-in-one pen system (Fig. 5e) where the body of the pen only contains a microcontroller, potentiostat, insulin pump, and Bluetooth module. Together these results confirm that we are able to incorporate a disposable glucose sensor on the tip of the insulin injection needle, usable in a custom insulin pen, capable of sensing the interstitial glucose concentration prior to calculation and delivery of an insulin dose. Although we have demonstrated these fully integrated systems, we acknowledge that future work is necessary to directly correlate the measured interstitial glucose concentration with blood glucose, and to develop standardized insertion protocol/workflow to further improve stabilization time and measurement precision for future translation of the all-in-one needle device. Moreover, the all-in-one needle may in the future be adapted for integrated glucose sensing and delivery in combined CGM/insulin pump based systems, though further long-term characterization is needed to determine how bolus insulin delivery near the glucose sensing location would change measured glucose sensing of the system.

3.7. Time analysis of ease of use

After the detailed introduction of the automated carbohydrate counting system and the two all-in-one insulin delivery systems, we provide here a brief comparison of the time expenditure for calculation of carbohydrate coverage and high blood sugar correction for a pre-prandial insulin dose calculation and delivery between the conventional approach, the all-in-one vacuum/strip pen, and the all-in-one needle pen. Our food carbohydrate estimation system can not only replace the numerous food portion size estimation and carbohydrate calculation methods currently used, but is also more time-saving for patients as they only need to take a photo of the meal with their smartphone. Fig. 6a shows the time analysis results of using the conventional approach and the computer vision-based approach. In order to achieve similar accuracy as the computer vision-based one, the conventional one from patients needed a much longer time and the time varied from person to person, which largely depends on how familiar they are with the food types. While our system takes typically 10 s to process the image, including uploading data to our server for food recognition and obtaining the food carbohydrate information from the Calorie Mama API.

For high blood sugar correction, the conventional approach is sophisticated and time-consuming and requires the patients to adopt multiple separate procedures based on current standard of care guidelines (46). We demonstrate these time-consuming and sophisticated procedures can be greatly simplified by using all-in-one systems. Although the all-in-one vacuum/strip pen still requires the users to assemble a lancet, testing strip, and insulin needle, the automated procedures for collecting blood sample, measuring blood glucose level, and delivering insulin not only reduce the complexity for dosing insulin but also results in a 50% reduction in time compared to standard procedures (Fig. 6b). The blood extraction time of the vacuum-based all-in-one system includes the vacuum for skin stretching, lancing the skin, and waiting for blood feeding into testing strip. The insulin dose calculation for both the two all-in-one pens includes glucose measurement and insulin dose conversion. The insulin delivery time includes the needle injection and insulin pumping time. Moreover, the all-in-one needle further removes the need for blood sampling, which furthermore decreases workflow time. Both all-in-one pens only require a single manual step from the user to realize the pre-prandial insulin delivery; for the all-in-one vacuum/strip pen, the user needs to place the pen onto a desired site for blood sampling and insulin delivery; for the all-in-one needle pen, the user only needs to insert the needle into a desired area for insulin delivery. These fully automated procedures also remove the time uncertainty in each manually handled procedure in the conventional approach. The large time variation in the insulin delivery of both the all-in-one systems comes from the variation in the required insulin units for delivery which requires 2 s to deliver 1 unit of insulin (Supplementary Fig. 6a).

4. Conclusion

According to the American Diabetes Association, diabetes technology, together with patient education and medical follow-up, can improve the lives and health of people with diabetes (14). In this work, we have developed an “all-in-one” system incorporating a smartphone application for computer vision-enabled carbohydrate counting with an “all-in-one” insulin pen containing a blood glucose measurement and insulin delivery system. We showcase two separate versions of the “all-in-one” pen, the first of which combines existing devices of test strip, lancet, glucometer and insulin pen that are familiar to patients into one

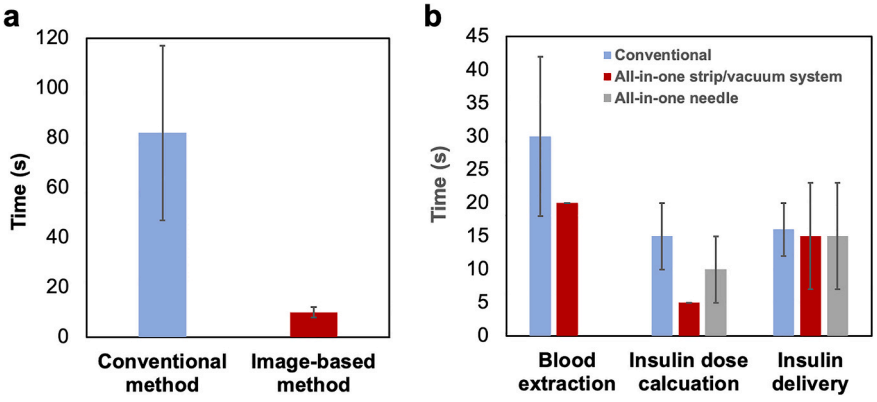

Fig. 6. Time analyses of pre-prandial insulin delivery using the conventional approach, all-in-one strip/vacuum system, and the all-in-one needle system. (a) Time required for estimating intake carbohydrate. (b) Time required for glucose measurement and insulin delivery. Each method and procedure were tested three times.

easy to use package, and the second of which shows the proof of concept for an "all-in-one" needle that can both measure and deliver insulin with only one needle injection. The main goal of the all-in-one system is to simplify the multiple sophisticated manual procedures for safe insulin delivery by automating the carbohydrate estimation, blood glucose measurement, insulin dose calculation, and insulin delivery. Furthermore, we demonstrate the feasibility of using a single needle for measuring glucose and delivering insulin, which in turn eliminates the notoriously painful blood sampling using a lancet. Our primary targets for these devices are patients who use insulin pen/test strip-based systems to manage diabetes. While patients who are using continuous glucose monitoring would not directly benefit from the glucose measurement capabilities of the all-in-one pen system, they can still use the carbohydrate counting system to combine with their blood glucose measurement from the CGM to facilitate insulin dose calculation. Furthermore, the all-in-one glucose measurement can also be used to cross-validate the blood glucose values measured on the CGM system. These technologies together have significant potential to reduce the patient burden of diabetes management and improve adherence to delivering an accurate pre-prandial and correction insulin dose, which consequently enhances patient health outcomes.

Supplementary data to this article can be found online at https://doi.org/10.1016/j.jconrel.2022.01.001.

Author contributions

G.T. and F.H. delineated the general area and unmet need. H.-W. H., S.S.Y., and G.T. designed the study including general concepts, H.-W. H., S.Y., L.D.T, and C.L. performed the experiment and analyzed the data. E. R., A.W., I.B., D.G., and K.N. supported prototyping of all-in-one pen systems. F.H. contributed to the functional requirements of the systems. C.E., C.L., and H.-W. H. developed and evaluated computer vision algorithms for carbohydrate counting. C.S., Ju.L., J.Y.L., Ja.L., and J.D.B. supported evaluation of the pen systems ex vivo and in vivo. J.C., S.T., and K.I. performed pig experiments with devices developed here. All authors contributed to writing of the manuscript.

Data and materials availability

All data associated with this study are present in the paper and/or the Supplementary Materials.

Declaration of Competing Interest

H.-W. H., S.S.Y., L.D.T., C.L. and G.T. declare submission of provisional patent application (Provisional Patent Application 63/183,451) describing the materials and applications of the systems described here. C.S. is employed by Bayer Pharmaceuticals. Complete details of all relationships for profit and not for profit for G.T. can be found at the following link:

www.dropbox.com/sh/szi7vnr4a2ajb56/AABs5N5i0q9AfT1IqIJAE-T5a?dl=0. All other authors declare that they have no competing interests.

Acknowledgements

This work was financially supported by the Karl van Tassel (1925) Career Development Professorship and the Department of Mechanical Engineering, Massachusetts Institute of Technology and discretionary funds from Brigham and Women's Hospital (G.T.). We are thankful to Mr. Mohammedali Roowala for his assistance in the fabrication of the first prototype and Mr. George Seisling for electronics related assistance.

References

[1] National Diabetes Statistics Report, | CDC, 2020 available at, https://www.cdc.gov/diabetes/library/features/diabetes-stat-report.html.
[2] Diabetes (available at https://www.who.int/health-topics/diabetes#tab=tab_1).
[3] Leading causes of death worldwide 2019 | Statista (available at https://www.statista.com/statistics/288839/leading-causes-of-death-worldwide/).
[4] E. Selvin, C.M. Parrinello, N. Daya, R.M. Bergenstal, Trends in insulin use and diabetes control in the U.S.: 1988–1994 and 1999-2012, Diabetes Care 39 (2016) e33–e35.
[5] K.J. Lipska, X. Yao, J. Herrin, R.G. McCoy, J.S. Ross, M.A. Steinman, S.E. Inzucchi, T.M. Gill, H.M. Krumholz, N.D. Shah, Trends in drug utilization, glycemic control, and rates of severe hypoglycemia, 2006-2013, Diabetes Care 40 (2017) 468–475.
[6] Intensive Insulin Therapy :: Diabetes Education Online (available at https://dtc.ucsf.edu/types-of-diabetes/type1/treatment-of-type-1-diabetes/medications-and-therapies/type-1-insulin-therapy/intensive-insulin-therapy/).
[7] Insulin Administration, Diabetes Care 27 (2004) S106–S107.
[8] M.B. Christensen, N. Serifovski, A.M.H. Herz, S. Schmidt, E. Hommel, L. Raimond, H. Perrild, A. Gotfredsen, P. Gæde, K. Nørgaard, Efficacy of bolus calculation and advanced carbohydrate counting in type 2 diabetes: a randomized clinical trial, Diabetes Technol. Ther. 23 (2021) 95–103.
[9] E. Hommel, S. Schmidt, D. Vistisen, K. Neergaard, M. Gribhild, T. Almdal, K. Nørgaard, Effects of advanced carbohydrate counting guided by an automated bolus calculator in type 1 diabetes mellitus (StenoABC): a 12-month, randomized clinical trial, Diabet. Med. 34 (2017) 708–715.
[10] J. Krzymien, P. Ladyzynski, Insulin in type 1 and type 2 diabetes—should the dose of insulin before a meal be based on glycemia or meal content? Nutrients 11 (2019) https://doi.org/10.3390/nu11030607.
[11] FDA approves first continuous glucose monitoring system for adults not requiring blood sample calibration | FDA (available at https://www.fda.gov/news-events/press-announcements/fda-approves-first-continuous-glucose-monitoring-system-adults-not-requiring-blood-sample).
[12] L. Van Den Boom, B. Karges, M. Auzanneau, B. Rami-Merhar, E. Lilienthal, S. Von Sengbusch, N. Datz, C. Schroder, T. Kapellen, M. Laimer, S. M. Schmid, H. Muller, J. Wolf, R. W. Holl, in Diabetes Care, (American Diabetes Association Inc., 2019), vol. 42, pp. 2050–2056.
[13] J.R. Petrie, A.L. Peters, R.M. Bergenstal, R.W. Holl, G.A. Fleming, L. Heinemann, Improving the clinical value and utility of CGM systems: Issues and recommendations a joint statement of the European association for the study of diabetes and the American diabetes association diabetes technology working groupDiabetes Care 40, 2017, pp. 1614–1622.
[14] A.D. Association, 7. Diabetes Technology: Standards of Medical Care in Diabetes-2020Diabetes Care 43, 2020, pp. S77–S88.
[15] F.M. Cameron, T.T. Ly, B.A. Buckingham, D.M. Maahs, G.P. Forlenza, C.J. Levy, D. Lam, P. Clinton, L.H. Messer, E. Westfall, C. Levister, Y.Y. Xie, N. Baysal, D. Howsmon, S.D. Patek, B.W. Bequette, Closed-loop control without meal announcement in type 1 diabetes, Diabetes Technol. Ther. 19 (2017) 527–532.
[16] G.E. Umpierrez, D.C. Klonoff, Diabetes technology update: use of insulin pumps and continuous glucose monitoring in the hospital, Diabetes Care 41 (2018) 1579–1589.
[17] P. Lasalvia, J.E. Barahona-Correa, D.M. Romero-Alvernia, S. Gil-Tamayo, C. Castañeda-Cardona, J.G. Bayona, J.J. Triana, A.F. Laserna, M. Mejía-Torres, P. Restrepo-Jimenez, J. Jimenez-Zapata, D. Rosselli, Pen devices for insulin self-Administration compared with needle and vial: systematic review of the literature and Meta-AnalysisJ, Diabetes Sci. Technol. 10 (2016) 959–966.
[18] T.S. Bailey, J.Y. Stone, A novel pen-based Bluetooth-enabled insulin delivery system with insulin dose tracking and advice, Expert Opin. Drug Deliv. 14 (2017) 697–703.
[19] GitHub - Frost-Lee/insulin_calculator: A system that calculates insulin dose by estimating carbs in a meal. (available at https://github.com/Frost-Lee/insulin_calculator).
[20] S.N. Mehta, N. Quinn, L.K. Volkening, L.M.B. Laffel, Impact of carbohydrate counting on glycemic control in children with type 1 diabetes, Diabetes Care 32 (2009) 1014–1016.
[21] A.S. Brazeau, H. Mircescu, K. Desjardins, C. Leroux, I. Strychar, J.M. Ekoé, R. Rabasa-Lhoret, Carbohydrate counting accuracy and blood glucose variability in adults with type 1 diabetes, Diabetes Res. Clin. Pract. 99 (2013) 19–23.
[22] Carb counting for diabetes: How to count and use the glycemic index (available at https://www.medicalnewstoday.com/articles/317267).
[23] A. Agianniotis, M. Anthimopoulos, E. Daskalaki, A. Drapela, C. Stettler, P. Diem, S. Mougiakakou, GoCARB in the context of an artificial pancreas, J. Diabetes Sci. Technol. 9 (2015) 549–555.
[24] D. Rhyner, H. Loher, J. Dehais, M. Anthimopoulos, S. Shevchik, R.H. Botwey, D. Duke, C. Stettler, P. Diem, S. Mougiakakou, Carbohydrate estimation by a Mobile phone-based system versus self-estimations of individuals with type 1 diabetes mellitus: a comparative study, J. Med. Internet Res. 18 (2016), e101.
[25] S.P. Yang, Y.H. Seo, J.B. Kim, H. Kim, K.H. Jeong, Optical MEMS devices for compact 3D surface imaging cameras, Micro Nano Syst. Lett. 7 (2019) 8.
[26] W. Boonsuk, Investigating effects of stereo baseline distance on accuracy of 3D projection for industrial robotic applications, 5th IAJC/ISAM Jt, Int. Conf. 9 (2016).
[27] Calorie Mama Food AI - Food Image Recognition and Calorie Counter using Deep Learning (available at https://www.caloriemama.ai/#CalorieMama).
[28] Food Nutrition Facts and Free Calorie Counter | CalorieKing (available at https://www.calorieking.com/us/en/).

[29] D.D. Cunningham, T.P. Henning, E.B. Shain, D.F. Young, T.A. Elstrom, E.J. Taylor, S.M. Schroder, P.M. Gatcomb, W.V. Tamborlane, Vacuum-assisted lancing of the forearm: an effective and less painful approach to blood glucose monitoring, Diabetes Technol. Ther. 2 (2000) 541–548.
[30] D.D. Cunningham, T.P. Henning, E.B. Shain, D.F. Young, J. Hannig, E. Barua, R. C. Lee, Blood extraction from lancet wounds using vacuum combined with skin stretching, J. Appl. Physiol. 92 (2002) 1089–1096.
[31] U. Jacobi, M. Kaiser, R. Toll, S. Mangelsdorf, H. Audring, N. Otberg, W. Sterry, J. Lademann, Porcine ear skin: an in vitro model for human skin, Skin Res. Technol. 13 (2007) 19–24.
[32] A. Pfützner, C. Schipper, S. Ramljak, F. Flacke, J. Sieber, T. Forst, P.B. Musholt, Evaluation of the effects of insufficient blood volume samples on the performance of blood glucose self-test meters, J. Diabetes Sci. Technol. 7 (2013) 1522–1529.
[33] Genteel Lancing Device -Give fingers a break when checking blood sugar (available at https://www.mygenteel.com/).
[34] Calculating Bolus Injections (available at https://www.nationwidechildrens.org/family-resources-education/health-wellness-and-safety-resources/resources-for-parents-and-kids/managing-your-diabetes/chapter-seven-calculating-bolus-injections).
[35] How To Inject Insulin (available at https://www.diabetes.co.uk/insulin/how-to-inject-insulin.html).
[36] Insulin Pen Injections Procedure Details | Cleveland Clinic (available at https://my.clevelandclinic.org/health/treatments/17923-insulin-pen-injections/procedure-details).
[37] A. Serafin, M. Malinowski, A. Prażmowska-Wilanowska, Blood volume and pain perception during finger prick capillary blood sampling: are all safety lancets equal? Postgrad. Med. 132 (2020) 288–295.
[38] X. Yu, H. Wang, X. Ning, R. Sun, H. Albadawi, M. Salomao, A.C. Silva, Y. Yu, L. Tian, A. Koh, C.M. Lee, A. Chempakasseril, P. Tian, M. Pharr, J. Yuan, Y. Huang, R. Oklu, J.A. Rogers, Needle-shaped ultrathin piezoelectric microsystem for guided tissue targeting via mechanical sensing, Nat. Biomed. Eng. 2 (2018) 165–172.
[39] T.R. Ray, J. Choi, A.J. Bandodkar, S. Krishnan, P. Gutruf, L. Tian, R. Ghaffari, J. A. Rogers, Bio-integrated wearable systems: a comprehensive review, Chem. Rev. 119 (2019) 5461–5533.
[40] J.Y. Oh, Z. Bao, Second skin enabled by advanced electronics, Adv. Sci. 6 (2019), https://doi.org/10.1002/advs.201900186.
[41] G. Schiavone, S.P. Lacour, Conformable bioelectronic interfaces: mapping the road ahead, Sci. Transl. Med. 11 (2019) 1–4.
[42] Continuous Glucose Monitoring System | FreeStyle Libre System (available at https://www.freestylelibre.us/).
[43] Dexcom G6 Continuous Glucose Monitoring (CGM) System | Zero Fingersticks (available at https://www.dexcom.com/g6-cgm-system).
[44] E. Cengiz, W.V. Tamborlane, A tale of two compartments: interstitial versus blood glucose monitoring, Diabetes Technol. Ther. 11 (2009), https://doi.org/10.1089/dia.2009.0002.
[45] N.A. Morris, M.F. Cardosi, B.J. Birch, A.P.F. Turner, An electrochemical capillary fill device for the analysis of glucose incorporating glucose oxidase and ruthenium (III) hexamine as mediator, Electroanalysis 4 (1992) 1–9.
[46] D. Pickering, J. Marsden, How to measure blood glucoseCommunity eye heal, J. 27 (2014) 56–57.